dc signal detection via dynamical asymmetry in a nonlinear device

M. E. Inchiosa* and A. R. Bulsara†
Space and Naval Warfare Systems Center San Diego, Code D364, San Diego, California 92152-6171
(Received 8 January 1998)

We study the detection of very small changes in a ''target'' dc signal, using a nonlinear dynamic sensor that is ac biased with a *known* sinusoidal signal. The sensor's nonlinear response generates harmonics at the odd multiples of the ac bias frequency ω in the absence of the dc signal, and at *all* multiples of ω in the presence of the dc signal, with the spectral amplitudes of these harmonics being very sensitive to the dc signal amplitude. For weak ac bias amplitude we use perturbation theory to calculate signal and noise powers at dc, at the fundamental (at frequency ω), and at the first harmonic (at frequency 2ω), from which we can predict the signal detection statistics. We compare these results with numerical simulations for both weak and strong ac bias amplitudes, as well as with results for an optimal detector. As our example nonlinear dynamic sensor, we use an rf superconducting quantum interference device loop. [S1063-651X(98)13806-0]

PACS number(s): 05.40.+j, 02.50.Ey, 85.25.Dq

I. INTRODUCTION

Periodically modulated stochastic systems have received considerable attention recently [1]; these systems, which can generally be described by the ''particle-in-potential'' paradigm, $dx/dt = -\partial U(x)/\partial x + S(t) + N(t)$, exhibit a richness of noise-mediated resonance behavior in the spectral measures (e.g., the output signal-to-noise ratio, SNR) of the response. Here, $S(t)$ and $N(t)$ denote a deterministic signal (usually taken to be time periodic) and noise (usually taken to be Gaussian). If the potential energy function $U(x)$ is even (often bistable), then the output power spectral density (PSD) consists of a Lorentzian-like noise background with peaks appearing at the *odd* multiples of the signal frequency ω. However, real-world manifestations of these systems are often asymmetric, with the dynamics containing even and odd functions of the state variable. The simplest route to asymmetry in the above dynamics is to incorporate a small dc term x_0 into the signal $S(t)$ or, equivalently, a term xx_0 into $U(x)$. The output PSD of asymmetric systems contains *all* the harmonics of the periodic signal frequency; hence, the appearance and magnitudes of the even multiples of ω could be taken as quantifying measures of the asymmetry-producing signal.

Asymmetric dynamic systems of the above form have been studied [2] with Gaussian white noise. The spectral amplitudes of the harmonics of the periodic signal, in the output PSD, pass through maxima as a function of noise variance. In recent work [3], we presented a systematic derivation of the resonant behavior of the spectral amplitudes of the harmonics at $k\omega$ ($k=1,2,3,\ldots$) in a generic nonlinear dynamical system subject to a weak symmetry-breaking dc signal in addition to a known cyclic signal. The resonant behavior was found to depend on a new control parameter, the degree of asymmetry, and was interpreted at all orders k, via a matching of deterministic (the frequency $k\omega$) and stochastic (the interstate hopping rate in the absence of the signal) time scales (the hopping rate depends critically on the asymmetry as well as the spectral characteristics of the noise) in the same manner as the ''standard'' stochastic resonance [1,4]. Calculations carried out on a specific nonlinear dynamic system, the rf superconducting quantum interference device (SQUID) loop subject to Gaussian *correlated* noise, demonstrated a remarkable agreement with numerical simulations within the framework of the perturbation-theory-based approximations inherent in the theory.

To determine whether the SR effect has signal processing applications, however, we cannot rely on SNR alone. For example, a nonlinear signal processor may output a signal that has infinite SNR but is useless because it has no correlation with the input signal. For signal estimation, relevant measures are mean square error or Bayesian tests [5]. For signal detection, one must consider detection statistics: probability of detection and probability of false alarm. Probability of detection is the probability that the system will report that a signal is present when in fact a signal *is* present. Probability of false alarm is the probability that the system will report that a signal is present when in fact a signal is *not* present. Such statistics are summarized in a plot of detection probability versus false alarm probability known as the receiver operating characteristic (ROC). In recent publications [6,7], we computed the ROCs for a single bistable element and a globally coupled array of such elements. The detection probability (for a fixed false-alarm rate) was found to follow the behavior of the output SNR: it displayed a maximum as a function of noise, and the coupling significantly enhanced signal detection performance over that obtained for a single element.

While SR does lead to an enhancement in the signal detection performance of an *a priori* nonlinear sensor, it generally cannot provide an output SNR in excess of the input SNR, when the input signal is a known, subthreshold signal in Gaussian noise. For this case, a nonlinear device will never outperform the (ideal) matched filter; however, in practice, such an ideal (linear) filter is often difficult to implement. One such example is afforded by the SQUID, which, despite being the most sensitive detector of magnetic fields, is severely limited by sensor-environmental noise in

*Electronic address: inchiosa@nosc.mil
†Electronic address: bulsara@nosc.mil

practical applications wherein it is operated in a feedback or ''flux-locked'' configuration [8]. SR has already been shown to occur in a single-junction (rf) SQUID [9]; hence, it offers the possibility of a constructive utilization of that portion of the noise that cannot be canceled by existing techniques. Recent theoretical studies [3] and experiments [10] indicate that the technique outlined above may be applicable to many nonlinear sensors that must detect weak dc signals in the presence of significant amounts of low frequency noise. By applying a *known* bias signal with carefully selected frequency ω, the detection may be shifted to a more acceptable part of the frequency spectrum. It is important to note that the technique should work best when the signals (the target and cyclic bias) are uncorrelated with the noise background; in practical signal detection scenarios, this is frequently the case. Then, in a detector that has an *a priori* symmetric potential, the appearance of the even multiples of ω in the output PSD, together with the change in their spectral amplitudes in the presence of the symmetry-breaking signal (which may be dc or monochromatic ac, in which case one looks at the properties of combination tones in the output PSD), may be used to detect or estimate the weak target signal. In remote sensing applications, one often knows *a priori* the spectral characteristics of the background noise as well as the sensor noise (in the absence of the signal); hence, one is afforded the possibility of optimizing the sensor parameters (specifically, the potential energy function) to achieve the best possible detection.

In this paper, we present a systematic computation of the signal detection statistics for the single-junction (rf) SQUID (which we take to be our example nonlinear dynamic device) subject to a weak dc target signal in the presence of ambient noise and a known cyclic (having frequency ω) bias signal. We consider the response at the frequencies $0,\omega,2\omega$ only, building on the results of our earlier publications [3]; however, in addition to the output signal power we must now compute the noise power as well. This calculation is carried out in Sec. III. We begin by briefly describing the rf SQUID loop and summarizing our earlier results [3].

II. THE rf SQUID LOOP

The standard rf SQUID loop is a superconducting loop into which a single Josephson junction has been inserted [8]. The dynamics are multistable with the magnetic flux through the superconducting loop being quantized in units of the flux quantum $\Phi_0 \equiv h/2e$. In the presence of the junction, the magnetic flux Φ through the loop, in response to an applied time-dependent magnetic flux Φ_e, evolves according to the dynamics [8],

$$\left(LC\frac{d^2}{dt^2} + \tau_L \frac{d}{dt} + 1 \right) \frac{\Phi(t)}{\Phi_0} + \frac{\beta_s}{2\pi} \sin \frac{2\pi\Phi(t)}{\Phi_0} = \frac{\Phi_e(t)}{\Phi_0}, \tag{1}$$

where L and C are the loop inductance and capacitance, $\tau_L \equiv L/R_J$ is the SQUID time constant (R_J being the normal state resistance of the junction), and the parameter $\beta_s \equiv 2\pi L i_c/\Phi_0$ (i_c is the junction critical current) controls the hysteretic behavior of the device. In most practical applications, the SQUID loop is shunted by a low resistance in order to remove hysteresis in the voltage-current characteristic of the junction [8]; this process effectively renders the link capacitance C extremely small so that the inertial term in Eq. (1) may be neglected. Transforming to the normalized state variable $x(t) \equiv \Phi(t)/\Phi_0$, we may write the dynamics (1) in the ''particle-in-a-potential'' form:

$$\tau_L \dot{x} = -\frac{\partial U(x)}{\partial x} + \eta(t) + y(t) \tag{2}$$

where the dot denotes time differentiation, and the potential function

$$U(x) = \frac{1}{2}(x - x_0)^2 - \frac{\beta_s}{4\pi^2} \cos 2\pi x \tag{3}$$

is multistable when $\beta_s > \beta_{sc}$, where $\beta_{sc} = 1$ for $x_0 = 0$. This multistability translates into a hysteretic, or multivalued, Φ versus Φ_e transfer characteristic. We have expressed the (normalized) external flux Φ_e/Φ_0 as the sum of three terms: a symmetry-breaking dc term x_0 [which we incorporate into $U(x)$], an ac term $\eta(t) = A\sin(\omega t + \theta)$ with θ being a (often assumed random) phase factor, and a noise term $y(t)$. Typically the time constant $\tau_L \approx 10^{-12}$ s, so that with the exception of the (internal) thermal noise, which is assumed negligible for the purposes of this paper, any externally applied noise will usually have a bandwidth far smaller than the SQUID bandwidth τ_L^{-1}. This is even more the case in experimental setups wherein a resistive shunt must often be placed across the SQUID to filter out high-frequency noise. The LR circuit formed by the shunt resistance and the loop inductance results in a low-pass filter that decreases the input noise bandwidth even further [9]. Hence we must take $y(t)$ to be zero-mean Gaussian *exponentially correlated* noise; it may be modeled via a white-noise-driven Ornstein-Uhlenbeck (O-U) process [11]:

$$\dot{y} = -\tau_c^{-1} y + \sigma F(t), \tag{4}$$

where $F(t)$ is zero-mean ''white'' noise with autocorrelation $\langle F(t)F(t+s)\rangle_t = \delta(s)$ and τ_c is the correlation time of the ''colored'' noise $y(t)$. Then, one easily verifies [11] that $y(t)$ has zero mean and autocorrelation function $\langle y(t)y(t+s)\rangle_t = \langle y^2\rangle e^{-|s|/\tau_c}$, whence the ''white'' limit, corresponding to delta-correlated noise, is realized when $\tau_c \to 0$. The colored noise has variance $\sigma_y^2 \equiv \langle y^2\rangle = \sigma^2\tau_c/2$ [we reiterate that $y(t)$ has units of normalized magnetic flux].

It is convenient to prebias the SQUID loop so that the potential (3), for the multistable case $\beta_s > \beta_{sc}$, is centrally bistable with possible outlying metastable states. This is accomplished [9] by incorporating a dc bias $m/2$ (m odd) in the potential: we replace x_0 by $x_0 + m/2$. Assuming the signal and noise to be very slow compared to the well-relaxation time (the standard adiabatic assumption), we may incorporate the signal $\eta(t)$ and the noise $y(t)$ into the potential function $U(x)$ as well, writing Eq. (2) in the form $\tau_L \dot{x} = -\partial U_e(x)/\partial x$ where the potential function U_e is now given by

$$U_e(x(t))=\frac{1}{2}\left(x-x_0-\frac{m}{2}-y(t)-\eta(t)\right)^2-\frac{\beta_s}{4\pi^2}\cos 2\pi x. \tag{5}$$

In this work, we consider the signal detection performance of the SQUID in its multistable, or dissipative, mode ($\beta_s>\beta_{sc}$). In this case, one treats the SQUID as a near-discrete hysteretic two-state system, with a transition rate between states; the rate can be readily calculated for the case of ''strongly'' (compared to the SQUID time constant) colored noise that is germane to the device: $\tau_c\gg\tau_L$. This procedure will be summarized in the following section, where we extend the calculations of [3] to compute the noise component in the output PSD of the device. We note that in recent work [12], we have considered the response (quantified by the output SNR at the fundamental of the known cyclic bias signal) of the rf SQUID operated in its nonhysteretic, or dispersive mode ($\beta_s\leqslant\beta_{sc}$), and subjected to a target dc signal. For this monostable potential case, the two-state approximation and the transition rate approach no longer apply. Instead, the output power spectral density (PSD) may be computed directly from an input-output transfer characteristic. Again, we obtain very good agreement with experiment.

It is important to note that the ''adiabatic assumption'' whereby we assume the SQUID to be a ''static nonlinearity'' subject to a signal of frequency far smaller than the SQUID bandwidth τ_L^{-1}, is critical to our ability to carry out the current as well as earlier [3,12] calculations. The assumption holds as long as $f(=\omega/2\pi)\ll\tau_L^{-1},\tau_c^{-1}$. In addition, we have made the above-mentioned assumption of strongly correlated external noise having correlation time $\tau_c\gg\tau_L$; the sensor's thermal noise (which is, in fact, broadband [8]) is assumed to be far smaller than the ambient or ''source'' noise, and will be neglected throughout. To summarize, we require $f\ll\tau_c^{-1}\ll\tau_L^{-1}$. We also assume that the signal and noise amplitudes are sufficiently low (the assumption of ''no deterministic switching'' a cornerstone of the current and previous [3] calculations) so that the SQUID may, in fact, be regarded as a centrally bistable system, in which the noise drives the dynamics between the two central (stable) minima of the potential, with excursions to the outlying metastable states occurring very seldom. Finally we note that our characterization of the SQUID as a device that usually resides in its steady state (this is predicated by the small time constant τ_L) implies that we may reduce the problem of the SQUID response to that of tracking the dynamics of the noise as it passes through the SQUID loop in the presence of the asymmetrizing dc flux and a slowly varying (known) cyclic signal that modulates or ''rocks'' the potential. Transition rates W_{12},W_{21} (these were computed in [3] and will be discussed again below) characterize the ''hopping'' between the allowed SQUID states of the noise variable, and one requires the adiabatic condition $f\ll W_{12},W_{21}$ for our characterization of the SQUID as a static nonlinearity with dichotomous Markovian dynamics to be valid. This condition sets a lower limit on the values of noise variance σ_y^2 that satisfy our theoretical assumptions.

III. OUTPUT POWER SPECTRUM; SIGNAL POWER AND NOISE POWER

In [3] we calculated, for an asymmetric potential, the response power at the fundamental ω and first harmonic 2ω of the cyclic drive frequency. In this paper we first derive the noise power spectrum by adapting the approach of [13] to apply to an asymmetric potential. To accomplish this, we extend [13] to second order in perturbation theory. For the signal power at ω and 2ω, we recover the results of [3]. Note that terms for the signal power at twice the driving frequency first appear in second order perturbation theory. However, for the noise power, first order perturbation theory is sufficient (for sufficiently weak driving). We can use the second order terms to test whether we have exceeded the limits of the first order result.

We model the SQUID as a two-state system with state probabilities $p_{1,2}(t)$ that evolve via the master equations [3]

$$\begin{aligned}\dot{p}_1&=W_{21}p_2-W_{12}p_1,\\ \dot{p}_2&=W_{12}p_1-W_{21}p_2,\end{aligned} \tag{6}$$

where $p_1+p_2=1$ and W_{ik} denotes the transition rate from state i to state k. The master equations (6) have the solution [13]

$$\begin{aligned}p_1(t)&=g^{-1}(t)\left[p_1(t_0)g(t_0)+\int_{t_0}^{t}W_{21}(t')g(t')dt'\right],\\ g(t)&=\exp\left\{\int^{t}[W_{12}(t')+W_{21}(t')]dt'\right\}.\end{aligned} \tag{7}$$

We can integrate Eq. (7) if we carry out a perturbation-theoretic expansion of the transition rates to second order in an expansion parameter $A'(\equiv A/\sqrt{2\sigma_y^2})\ll 1$:

$$\begin{aligned}W_{12}&\approx\alpha_0+\alpha_1\eta'(t)+\alpha_2\eta'^2(t),\\ W_{21}&\approx\beta_0+\beta_1\eta'(t)+\beta_2\eta'^2(t),\end{aligned} \tag{8}$$

where $\eta'(t)\equiv A'\sin(\omega t+\theta)$. The expansion coefficients are obtained through a straightforward Taylor expansion of the transition rates, and they may be found in [3].

Using the transition rate expansion (8), we can integrate (7) to obtain the probability that the particle is in the ''1'' state at time t given that it was in the s_0 state at time t_0 (where $s_0\in\{1,2\}$). Collecting terms in powers of the expansion parameter A', we obtain

$$p_1(t|s_0,t_0)=p_{10}+A'p_{11}+A'^2p_{12}+O(A'^3), \tag{9}$$

where the coefficients are

$$p_{10}=\frac{\alpha-\overline{\alpha}}{2\alpha}+e^{-\alpha(t-t_0)}\frac{(2\delta_{s_01}-1)\alpha+\overline{\alpha}}{2\alpha}, \tag{10}$$

$$p_{11}=c_1a_1\cos(\omega t)+c_1b_1\sin(\omega t)+e^{-\alpha(t-t_0)}[b_2\sin(\omega t)+c_3a_3\cos(\omega t_0)+c_3b_3\sin(\omega t_0)], \tag{11}$$

and

$$p_{12}=C_1+c_4a_4\cos(2\omega t)+c_4b_4\sin(2\omega t)+e^{-\alpha(t-t_0)}\{C_2+C_3(t-t_0)+c_5\sin(\omega t)[a_5\cos(\omega t_0)+b_5\sin(\omega t_0)]+c_6a_6\cos(2\omega t)$$
$$+c_6b_6\sin(2\omega t)+c_7a_7\cos(2\omega t_0)+c_7b_7\sin(2\omega t_0)\}. \tag{12}$$

The a's, b's, c's, and C's depend only on the Kronecker δ function δ_{s_01}, the ac bias frequency ω, and the expansion coefficients in Eq. (8); we list their definitions in the Appendix. For convenience, we have also switched to the sum and difference variables $\alpha\equiv\alpha_0+\beta_0$, $\beta\equiv\alpha_1+\beta_1$, $\gamma\equiv\alpha_2+\beta_2$, $\overline{\alpha}\equiv\alpha_0-\beta_0$, $\overline{\beta}\equiv\alpha_1-\beta_1$, and $\overline{\gamma}\equiv\alpha_2-\beta_2$.

In our two-state approximation, the probability density function of the SQUID output is

$$P(x,t)\approx p_1(t)\,\delta(x-x_{10})+p_2(t)\,\delta(x-x_{20}), \tag{13}$$

where x_{10} and x_{20} are the locations of the minima of the unperturbed potential energy (3). Therefore, we can compute the autocorrelation $\langle x(t)x(t+\tau)|s_0,t_0\rangle$ from $p_1(t|s_0,t_0)$ using

$$\langle x(t)x(t+\tau)|s_0,t_0\rangle=[x_{10}p_1(t)+x_{20}p_2(t)][x_{10}p_1(t+|\tau|)+x_{20}p_2(t+|\tau|)]. \tag{14}$$

Following [13], we average the autocorrelation over one cycle of the periodic ac bias flux and then perform a Fourier transform to obtain the output power spectrum. To second order in perturbation theory, the power spectrum consists of delta-function peaks at $\Omega=0$, ω, and 2ω, superimposed on a smooth noise background:

$$\mathcal{S}(\Omega)=M_0^2\delta(\Omega)+\frac{M_1^2}{2}\delta(\Omega-\omega)+\frac{M_2^2}{2}\delta(\Omega-2\omega)+N(\Omega). \tag{15}$$

M_1 and M_2 were calculated in [3], and

$$M_0=\sqrt{2\pi\overline{c}}+\sqrt{2\pi}c\,\frac{|\alpha\overline{\alpha}(\alpha^2+\omega^2)+(A'^2/2)[-\alpha\beta(\alpha\overline{\beta}-\overline{\alpha}\beta)+(\alpha\overline{\gamma}-\overline{\alpha}\gamma)(\alpha^2+\omega^2)]|}{\alpha^2(\alpha^2+\omega^2)}, \tag{16}$$

where $c\equiv(x_{10}-x_{20})/2$ and $\overline{c}\equiv(x_{10}+x_{20})/2$.

The noise term in Eq. (15) can further be written as the expansion

$$N(\Omega)=N_0(\Omega)+N_2(\Omega)A'^2+O(A'^4), \tag{17}$$

where

$$N_0(\Omega)\equiv\frac{2c^2(\alpha^2-\overline{\alpha}^2)}{\alpha(\alpha^2+\Omega^2)} \tag{18}$$

and

$$N_2(\Omega)\equiv\frac{c^2}{\alpha(\alpha^2+\Omega^2)}\Bigg\{-\frac{(\alpha\overline{\beta}-\overline{\alpha}\beta)^2}{\alpha^2+\omega^2}+\frac{-\alpha^2[(\alpha^2-\overline{\alpha}^2)\gamma+2\overline{\alpha}(\alpha\overline{\gamma}-\overline{\alpha}\gamma)]+[\overline{\alpha}(\gamma\overline{\alpha}-\overline{\gamma}\alpha)+\alpha(\alpha\gamma-\overline{\alpha\gamma})]\Omega^2}{\alpha(\alpha^2+\Omega^2)}$$
$$+\frac{\beta[\alpha^3(\alpha\beta-\overline{\alpha\beta})+5\alpha^2\overline{\alpha}(\alpha\overline{\beta}-\overline{\alpha}\beta)-4\alpha(\alpha\beta-\overline{\alpha\beta})\Omega^2+\beta(\alpha^2-\overline{\alpha}^2)(\Omega^2+\omega^2)]}{[\alpha^2+(\Omega-\omega)^2][\alpha^2+(\Omega+\omega)^2]}\Bigg\}. \tag{19}$$

We have computed the term in A'^4 as well, but we omit it due to its length and the fact that within the regime of validity of the perturbation theory expansion it adds a negligible contribution.

The features of S, N, and $S+N$ will be discussed in the following section, where we concentrate on the thrust of this paper: the signal detection problem.

IV. SIGNAL DETECTION

We will concentrate on detecting a small change Δx_0 in the flux, since large flux changes can be detected without using SQUIDs, or by using SQUIDs in conventional operating modes [8]. If the noise level is too high to permit useful signal detection, it may be reduced by choosing a sufficiently

narrow frequency bin width, although this requires observing the signal for a longer time before making a detection decision.

To maximize dc signal detection performance, one would like to bias the SQUID onto an operating region where the response depends sensitively on the dc signal and where the response noise is small.

One can get a general feel for where the signal detection performance will be optimal by looking at plots of signal power and noise power versus x_0. However, to make quantitative predictions of the signal detection performance we can use a modified version of the approach we used in [7] to calculate the probability of detection P_d and probability of false alarm P_f.

We perform signal detection by measuring the output power l in a frequency bin of width $\Delta\omega$ centered at frequency Ω. We then compare our ''test statistic'' l to a ''decision threshold'' Θ. If the power exceeds the threshold, we report that the target signal is present; otherwise, we report that it is absent. (Under certain conditions to be discussed later, we see a *drop* in power when the target signal is present. In such cases, we simply reverse the conditions for reporting the presence and absence of the target signal.)

To predict the probability of detection and probability of false alarm, we need to know the probability distribution $P(l)$ of our test statistic l. Calculating $P(l)$ is difficult due to the nonlinear nature of our system. We can, however, approximate $P(l)$ by the probability distribution of the power at the output of a bandpass filter of passband bandwidth $\Delta\omega$ centered at frequency Ω, which is fed by a sinusoidal wave of amplitude $\sqrt{2E_r}$ in white Gaussian noise having power $\mathcal{N}$ over a bandwidth $\Delta\omega$. (Such a bandpass filter is indeed the optimal detector of a sinusoidal wave of unknown random, uniformly distributed phase in white Gaussian noise [15].) The probability that the power at the output of the filter will exceed a threshold Θ is $Q(\sqrt{2E_r/\mathcal{N}},\sqrt{2\Theta/\mathcal{N}})$ [15], where Marcum's Q function is

$$Q(\alpha,\beta)\equiv\int_{\beta}^{\infty} z\exp\left(-\frac{z^2+\alpha^2}{2}\right)I_0(\alpha z)dz \tag{20}$$

and I_0 is the modified Bessel function of the first kind and order zero. Using this approximate model of our test statistic's probability distribution, we obtain the following probabilities of detection and false alarm:

$$P_d=Q(\sqrt{2E_{r1}/\mathcal{N}_1},\sqrt{2\Theta/\mathcal{N}_1}), \tag{21}$$

$$P_f=Q(\sqrt{2E_{r0}/\mathcal{N}_0},\sqrt{2\Theta/\mathcal{N}_0}), \tag{22}$$

where the subscripts 1 and 0 refer to the hypotheses H_1 and H_0 of having the dc target signal Δx_0 present and absent, respectively. E_r is the mean response signal power in a frequency bin of width $\Delta\omega$ centered at the detector's center frequency $\Omega=0$, ω, or 2ω, and equals total signal power minus noise power. (Note, however, that for practical signal detection the noise power is typically much less than the signal power, making the difference between signal power and total power negligible.) We can calculate the response noise power $\mathcal{N}$ in the test statistic's frequency bin from the noise terms in the analytical expression for the PSD. In the case of simulations, we estimate the noise power by averaging the power in the frequency bins 4–$8\Delta\omega$ above and below (unless $\Omega=0$) the test statistic's frequency bin (which is centered at frequency Ω).

This model represents an improvement over the model we used in [7]. In the present case we use the signal power and noise power, rather than just their ratio. This allows us to account for additional nonlinear effects and more complicated detection scenarios. In the previous model [7], the output noise power was taken to be the same under both hypotheses H_0 and H_1, and the output signal power was taken to be nonzero only under hypothesis H_1. The present model takes into account the fact that the nonlinear response yields a different output noise power under the two hypotheses H_0 and H_1. The present model also allows for nonzero output signal power under hypotheses H_1 *and* H_0.

For comparison we will also calculate the optimal detection of a dc signal Δx_0 in exponentially correlated Gaussian noise $y(t)$ as defined via Eq. (4). We observe the received signal $r(t)$ over an observation interval $[0,T]$. In general, increasing the observation time T improves the detection performance, but it also increases the amount of time that must elapse before a detection decision is made.

We can map our problem onto a more general binary hypothesis-testing problem worked out in [14]: in hypothesis H_1, a signal $s_1(t)$ was present during the observation interval, and in hypothesis H_0, a signal $s_0(t)$ was present.

$$\begin{aligned} H_1:&\quad r(t)=s_1(t)+n(t),\\ H_0:&\quad r(t)=s_0(t)+n(t),\end{aligned} \tag{23}$$

where $0\leqslant t\leqslant T$ and $n(t)$ is zero mean Gaussian noise, which may be nonstationary. In our case,

$$s_1(t)=\Delta x_0,\quad s_0(t)=0. \tag{24}$$

The optimal detection statistic is

$$\begin{aligned} G=&\,\mathrm{Re}\int_0^T h_1^*(t)\left[r(t)-\frac{1}{2}s_1(t)\right]dt\\ &-\mathrm{Re}\int_0^T h_0^*(t)\left[r(t)-\frac{1}{2}s_0(t)\right]dt.\end{aligned} \tag{25}$$

The filter functions $\{h_i(t)\}$ are solutions of

$$\int_0^T R(t,t')h_i(t')dt'=s_i(t), \tag{26}$$

where $R(t,t')$ is the covariance of the noise $n(t)$. If $n(t)$ is stationary, then we can replace $R(t,t')$ by $R(t-t')$. If the stationary noise has a power spectrum that is a rational fraction, then a method exists to find the $\{h_i(t)\}$ that solve Eq. (26).

We need the probability density of the test statistic G to compute the detector performance. Since G is obtained from a linear operation on a Gaussian signal, it too is Gaussian, and its probability density is fully described by its mean and variance. The expectation values $\mathcal{E}_1(G)$ and $\mathcal{E}_0(G)$ under hypotheses H_1 and H_0, respectively, are

$$\mathcal{E}_1(G) = -\mathcal{E}_0(G) = \frac{1}{2}\int_0^T [h_1(t)-h_0(t)]^*[s_1(t)-s_0(t)]dt, \quad (27)$$

and the variance of G is

$$\sigma_G^2 = 2|\mathcal{E}_1(G)|. \quad (28)$$

Setting the noise covariance in Eq. (26) equal to the covariance function $R_y(\tau)$ of our stationary Gaussian noise $y(t)$, the filter functions $\{h_i(t)\}$ are given by [14]

$$h_i(t) = \frac{\tau_c}{2\sigma_y^2}\{-s_i''(t)+s_i(t)/\tau_c^2+[-s_i'(0)+s_i(0)/\tau_c]\delta(t) + [s_i'(T)+s_i(T)/\tau_c]\delta(t-T)\}, \quad 0 \leqslant t \leqslant T. \quad (29)$$

Substituting Eqs. (24) and (29) into Eq. (25) and using Eqs. (27) and (28) gives the optimal detector for our particular signals and noise,

$$G = \frac{\Delta x_0}{2\sigma_y^2}\left[\frac{1}{\tau_c}\int_0^T r(t)dt + r(0) + r(T)\right] - \frac{1}{2}\sigma_G^2, \quad (30)$$

and its variance

$$\sigma_G^2 = \frac{\Delta x_0^2}{2\sigma_y^2}(2 + T/\tau_c). \quad (31)$$

Since $T \gg \tau_c$, we can make the approximations

$$G \approx \frac{\Delta x_0}{2\sigma_y^2\tau_c}\int_0^T r(t)dt - \frac{1}{2}\sigma_G^2, \quad (32)$$

and

$$\sigma_G^2 \approx \frac{\Delta x_0^2 T}{2\sigma_y^2\tau_c}. \quad (33)$$

From Eq. (32) we see that we can optimally detect the dc signal by simply integrating the received signal over the observation interval and comparing this integrated value to a decision threshold G_t.

We can obtain the optimal detector's probability of detection for a given threshold G_t by integrating the (Gaussian) probability density function of G from G_t to infinity under the H_1 hypothesis (recall that the expectation value of G depends on the hypothesis), giving us a result in terms of the complementary error function, $\mathrm{erfc}(z) \equiv 1 - (2/\sqrt{\pi})\int_0^z e^{-t^2}dt$,

$$P_d^{\mathrm{opt}} = \frac{1}{2}\mathrm{erfc}\left(\frac{1}{\sqrt{2\sigma_G^2}}\left[G_t - \frac{\sigma_G^2}{2}\right]\right). \quad (34)$$

We can likewise obtain the probability of false alarm by performing the same integration under the H_0 hypothesis, giving

$$P_f^{\mathrm{opt}} = \frac{1}{2}\mathrm{erfc}\left(\frac{1}{\sqrt{2\sigma_G^2}}\left[G_t + \frac{\sigma_G^2}{2}\right]\right). \quad (35)$$

Using these formulas we can easily study the dependence of the detection statistics P_d^{opt} and P_f^{opt} on the noise parameters σ_y^2 and τ_c, the target signal strength Δx_0, and the observation time T. For example, suppose we want to determine the dependence of P_d^{opt} on one of these parameters, keeping P_f^{opt} fixed. Inverting Eq. (35), solving for the decision threshold G_t, and inserting the result into Eq. (34) yields

$$P_d^{\mathrm{opt}} = \frac{1}{2}\mathrm{erfc}[\mathrm{erfc}^{-1}(2P_f^{\mathrm{opt}}) - \sqrt{\sigma_G^2/2}], \quad (36)$$

where erfc^{-1} is the inverse function of erfc. Now, using our equation (33) for σ_G^2, we can plot the dependence of P_d^{opt} on σ_y^2, τ_c, Δx_0, or T.

In many cases the SQUID signal detection performance will show a parameter dependence closely mirroring the optimal detector. For example, we would expect both detectors to have a similar observation time dependence provided $T \gg 2\pi/\omega$.

V. NUMERICAL RESULTS OF THEORY AND SIMULATIONS

We will consider three cases of ac bias signal amplitude, $A=0$, $A=0.1$, and $A=0.56$. In the first two cases we can estimate the response power spectrum analytically. In the third case the ac bias signal is just below the ''deterministic switching threshold,'' i.e., the level of bias that would modulate the potential wells so much that during each cycle of modulation the left well and right well would alternately disappear. In this case we rely on simulations since our perturbation theory assumptions do not hold.

We first consider the case $A=0.1$. Figure 1 shows the output power at frequencies $\Omega=0$, ω, and 2ω. Note that ''$S+N$'' simply refers to the total power in the output power spectrum over a frequency range of width $\Delta\omega$ centered at frequency Ω, and ''N'' refers to the contribution to the total power in this frequency range due to noise terms only. We have plotted the results of binary-filtered simulations beside the theoretical predictions. The binary filter outputs a fixed positive or negative value depending on whether the SQUID's state point lies in the right or left potential well, respectively. Since the theory uses a two-state approximation, we expect it to give better agreement with the binary-filtered result. In fact, the theory shows excellent agreement with the simulations for this value of A.

Figure 2 shows the output powers for $A=0$. (Note that for $A=0$ the total power equals the noise power except at $\Omega=0$, where there is a difference due to the nonzero dc value.) In the $A=0$ case, we check for the effects of the nonperturbative approximations made in the theory. These include the two-state approximation and the adiabatic approximations $\omega^{-1} \gg \tau_c \gg \tau_L$ [15]. We can see from the figure that the nonperturbative approximations cause very little error in predicting the binary-filtered output powers.

Figure 3 shows the unfiltered output powers and the de-

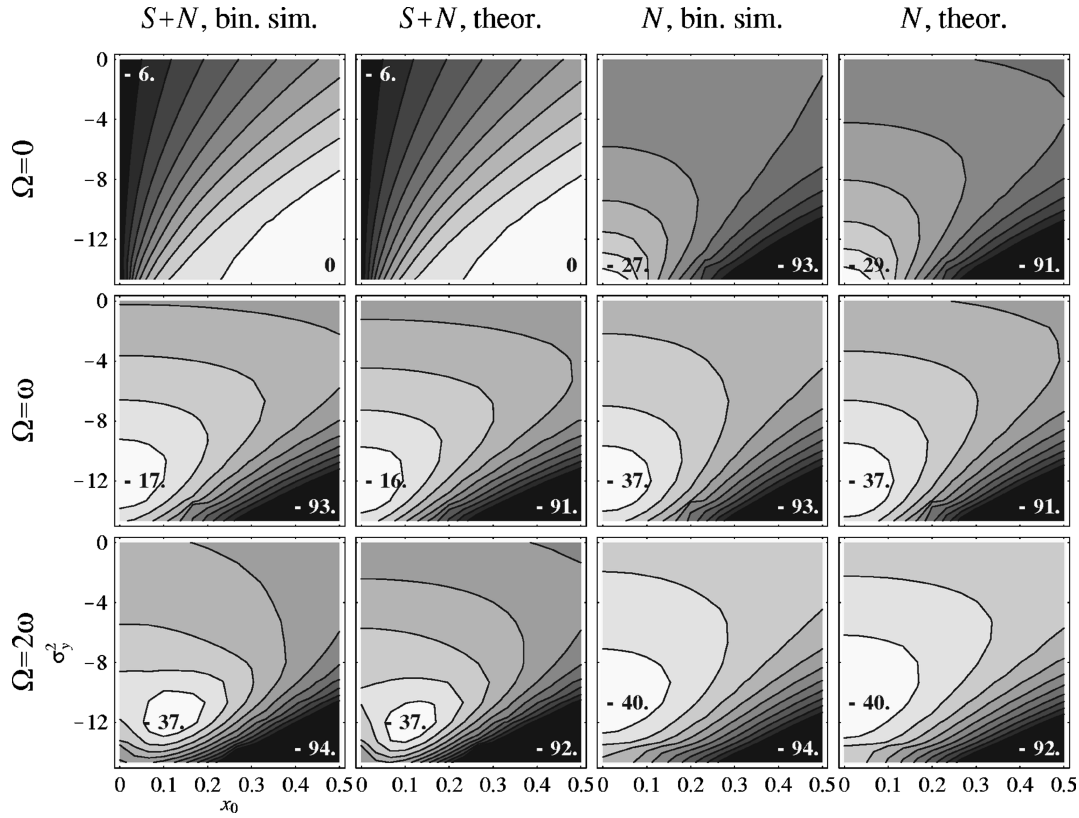

FIG. 1. Output power (in dB) at frequencies $\Omega=0$ (top row), ω (middle row), and 2ω (bottom row), computed as a function of dc bias x_0 in normalized units (see text) and noise variance σ_y^2 (in dB). Columns 1 and 2: total power computed via binary-filtered simulations and theory, respectively; column 3 and 4: noise power computed analogously. Numbers inside each frame denote the maximum and minimum powers (in dB). Parameter values: $A=0.1$, $\tau_c=0.01$, $T=161$ s, $\omega=10$, $\Delta\omega=\omega/256$, $\beta_s=5$.

tection probability P_d for a fixed false alarm probability of $P_f=0.1$. For $\Omega=\omega,2\omega$, the maximum P_d occurs close to the noise variance that maximizes the output power. However, the maximizing value of dc flux x_0 differs between the output power and P_d plots, since the rate of change of the output power with respect to the dc signal is zero at the maximum itself, and it is the variation of the output power with x_0 that makes detection possible. Note that for $\Omega=\omega$ the output power monotonically decreases as we increase x_0 from 0 to 0.5. Therefore, throughout this range of x_0's we can always do detection by looking for a drop in output power with increasing x_0. However, for $\Omega=2\omega$, the rate of change of the output power with x_0 can be positive or negative. Therefore, in the P_d plots for $\Omega=2\omega$ we plot the maximum detection probability using either a ''positive slope'' or a ''negative slope'' detector.

Each contour plot results from simulating the system at 208 different (x_0,σ_y^2) points. At each of the points we obtained the P_d ''sim.'' results by running 2048 numerical simulations each of the SQUID detector response with and without the dc target signal Δx_0 present. Each simulation involves generating long input and output time series (262 144 samples) and computing fast Fourier transforms. Due to the high computing demands, we ran our simulations in parallel using 128 processing elements of a Cray T3E supercomputer.

The contour plots labeled P_d ''mixed'' show predictions of P_d generated by employing a mixture of simulation and theory. First the system was simulated to obtain values of output signal power and noise power. Then these values were used in Eqs. (21) and (22) to obtain predictions of the detection probability P_d for a fixed false alarm probability of $P_f=0.1$. We could have dispensed with the simulation and used our theoretical expressions for the output signal power and noise power; however, the mixed approach allows us to isolate errors arising from the approximations used in the output power theory and the signal detection theory.

In Fig. 3 we showed the detection probability P_d only for a fixed false alarm probability $P_f=0.1$. Figure 4 shows curves of detection probability P_d *versus* false alarm probability P_f, known as ''receiver operating characteristics'' (ROCs). Different points along the ROCs correspond to different values of the decision threshold Θ. We show the results using a detector measuring total SQUID output power at frequency $\Omega=2\omega$, for the parameter values $x_0=0.2$, $\sigma_y^2=-13.33$ dB, which correspond to the maximum detection performance at 2ω. We find good agreement among the results obtained by simulation (solid curve), the mixture of simulation and theory discussed above (dashed curve), and the purely theoretical prediction (dotted curve).

Now we return to the case of zero ac bias amplitude ($A=0$). Even in the absence of an ac bias flux we can still detect the dc signal Δx_0 by its effect on the system's response to the input noise. We show the unfiltered output power and detection probability for this case in Fig. 5. Note that the maximum detection probabilities obtained for $\Omega=\omega,2\omega$ are lower than for the case $A=0.1$.

In Fig. 6 we plot the output powers and detection prob-

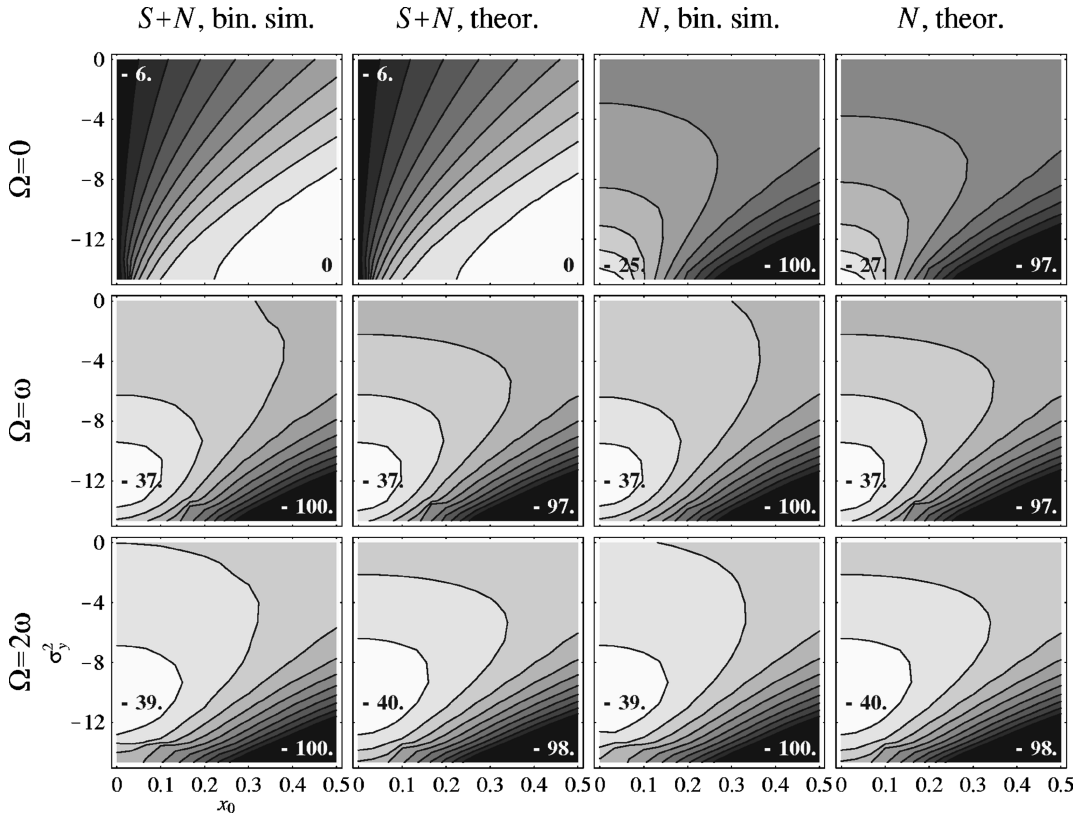

FIG. 2. Same as Fig. 1, with $A=0$.

ability for the *highly* nonlinear case $A=0.56$, as obtained by numerical simulation. Compared to the case $A=0.1$, the island of high output power in the first harmonic response ($\Omega=2\omega$) has become stretched to include lower input noise values. The maximum detection probability no longer occurs at the input noise variance that maximizes the output power. Also, the value of dc flux x_0 maximizing signal detection at $\Omega=2\omega$ occurs for x_0 close to zero, in contrast to the $A=0.1$ case.

Consider now the effect of changing τ_c, the colored noise correlation time. Comparing Figs. 3 and 7, we see that the output power maxima at $\Omega=\omega,2\omega$ shift to slightly smaller values of input noise variance as we decrease τ_c from 0.01 to 0.0005 (towards the limiting case of ''white'' noise). Note that the detection probabilities increase significantly. This is consistent with previous work [16] on the effects of colored noise on the output PSD and the SNR at $\Omega=\omega$; ''whitening'' the noise (i.e., decreasing the correlation time τ_c) leads to enhancement of the output SNR. Exceptions to this behavior do occur [17]; however, we do not discuss them here.

As we have noted earlier, optimal detection of the dc signal Δx_0 uses an ideal linear sensor to average the input signal over an observation interval and compares that average to a threshold. Figure 8 compares the optimal detector's performance (solid curve), calculated using Eq. (36), with the SQUID signal detection performance as measured via numerical simulation. We have plotted the detection probability P_d for a fixed false alarm probability of $P_f=0.1$, maximized over the dc bias x_0. The SQUID's ac bias flux amplitude is $A=0.1$. Using a detector measuring total output power at frequency $\Omega=0$ (diamonds), the SQUID detection performance matches the optimal detector. At frequency $\Omega=\omega$ (stars), the SQUID detection probability comes within 4% of the optimal detector for certain values of the noise variance. At $\Omega=2\omega$ (boxes), however, the SQUID performance suffers. Because the ac bias flux amplitude is well below the deterministic switching threshold, the SQUID's response is only weakly nonlinear, and not much power is generated at twice the ac bias frequency. Therefore, we see low signal detection performance using measurement at this frequency.

To improve the 2ω signal detection performance, we increased the ac bias flux amplitude to $A=0.56$, which is just below the deterministic switching threshold. This improved performance so much that we were also able to reduce the observation time from $T=161$ to $T=20.1$ sec and still get significant detection (Fig. 9). Comparing Figs. 8 and 9, we see that decreasing the observation time decreased the optimal detector's performance. Note, however, the *increase* in detection performance using the SQUID's output at $\Omega=2\omega$ (boxes). Even though the detection task has been made much more difficult by shortening the observation time, using a higher ac bias flux amplitude has more than compensated. In fact, the performance at $\Omega=2\omega$ now *exceeds* that at $\Omega=\omega$ (stars). Although the detection performance at $\Omega=0$ exceeds that at $\Omega=\omega,2\omega$, in practice it may be advantageous to detect at the higher frequencies due to the presence in the measurement system of additional noise sources having large amounts of low frequency energy, e.g., $1/f$ noise [18].

When applying our theory, we have stayed within the limits of validity of the perturbation approach embodied in our expansion of the transition rates in a power series in the parameter $A'=A/\sqrt{2\sigma_y^2}$. We have extended the computation of the noise power $N(\Omega)$ to $O(A'^4)$ and verified (not shown)

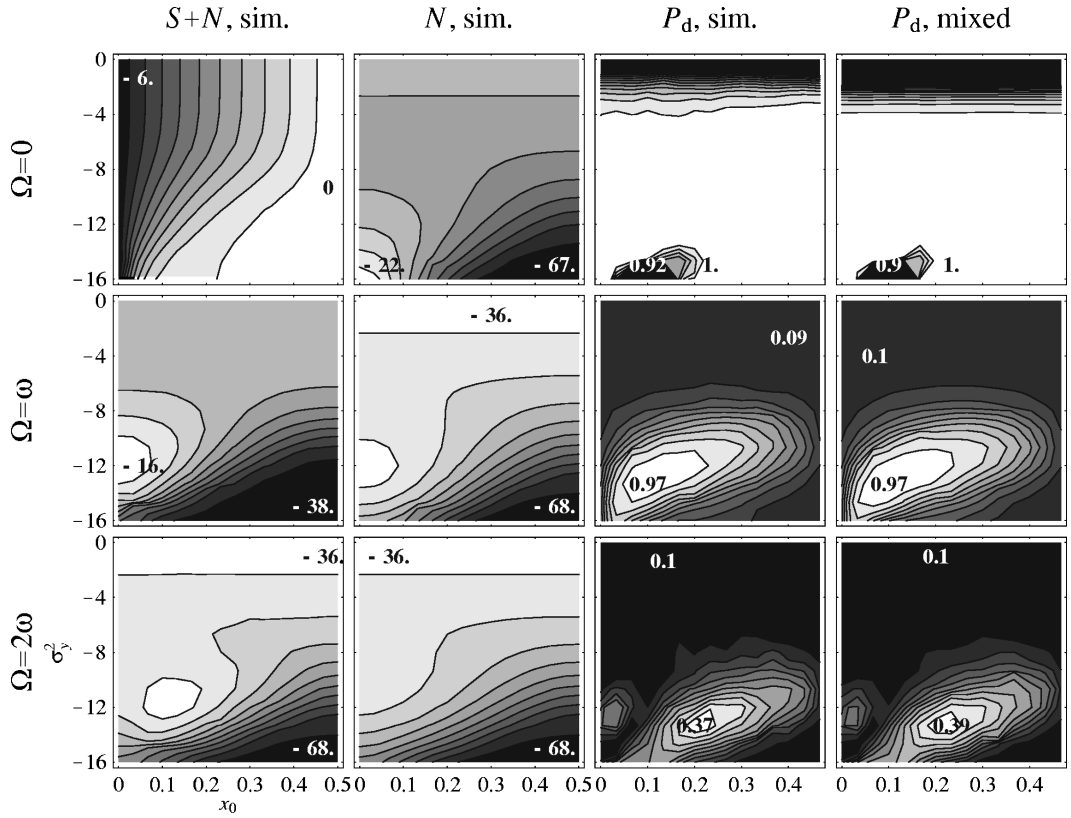

FIG. 3. Output power (in dB) and detection probability P_d at frequencies $\Omega=0$ (top row), ω (middle row), and 2ω (bottom row), plotted as a function of dc bias x_0 in normalized units (see text) and noise variance σ_y^2 (in dB). Columns 1 and 2: total power and noise power, respectively, computed via unfiltered simulations; column 3 and 4: detection probability P_d (at a fixed false alarm probability of $P_f=0.1$), computed via direct simulations and via a mixture of simulation and theory (see text), respectively. Numbers inside each frame denote the maximum and minimum powers (in dB), and the maximum and minimum probabilities. $\Delta x_0=0.0333$. Other parameter values: same as Fig. 1.

that the fourth-order term makes a negligible contribution to the noise power within the regime of validity of the perturbation expansion. Note, however, that for very *small* noise variances with the subthreshold signal strengths considered here, the perturbation theory breaks down; in fact, this parameter range corresponds to the strongly nonlinear regime wherein interesting phenomena (e.g., the appearance of dips in the output PSD) have been observed [19].

We conclude this section by summarizing the parameter ranges investigated. Starting with $A=0.1$, $\tau_c=0.01$, and $T=20.1$ s (not shown), we found that signal detection at $\Omega=\omega, 2\omega$ was quite poor. We increased the bias amplitude to $A=0.56$ (just below the deterministic switching threshold) and obtained very good detection. It is important to reiterate that in practical scenarios, the parameters A, ω, and T, would typically be under our control, whereas Δx_0, τ_c, and σ_y^2 would be imposed by the conditions of the experiment or application. To boost detection without approaching the deterministic switching threshold and thereby abandoning perturbation theory, we also tried increasing the observation time to $T=161$ s, while keeping $A=0.1$ and $\tau_c=0.01$; this yielded meaningful detection at $\Omega=\omega,2\omega$. Realizing that the quality of detection obtainable via the optimal detector increases with decreasing τ_c [see (33)], we were also able to improve signal detection considerably over the base case by reducing the noise correlation time to $\tau_c=0.0005$, while keeping $A=0.1$ and $T=20.1$ sec. The nonperturbative approximations were studied by setting $A=0$, using $\tau_c=0.01$ and $T=161$ s. We also note that the cyclic bias frequency ω should be carefully selected to stay within the framework of the adiabatic approximation that is central to the theoretical calculations of this work.

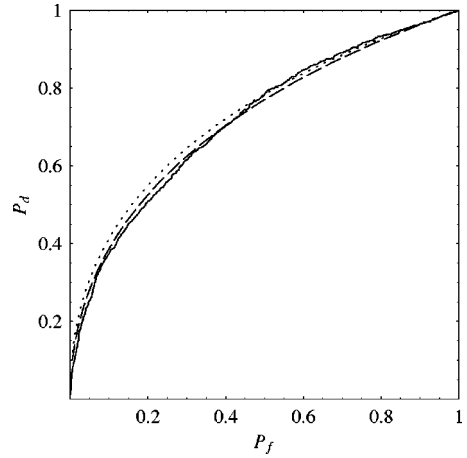

FIG. 4. Probability of detection P_d vs probability of false alarm P_f, using a detector measuring total SQUID output power at frequency $\Omega=2\omega$. Solid curve: simulation. Dashed curve: mixture of simulation and theory (see text). Dotted curve: purely theoretical prediction. $x_0=0.2$, $\sigma_y^2=-13.33$ dB. Other parameter values: same as Fig. 3.

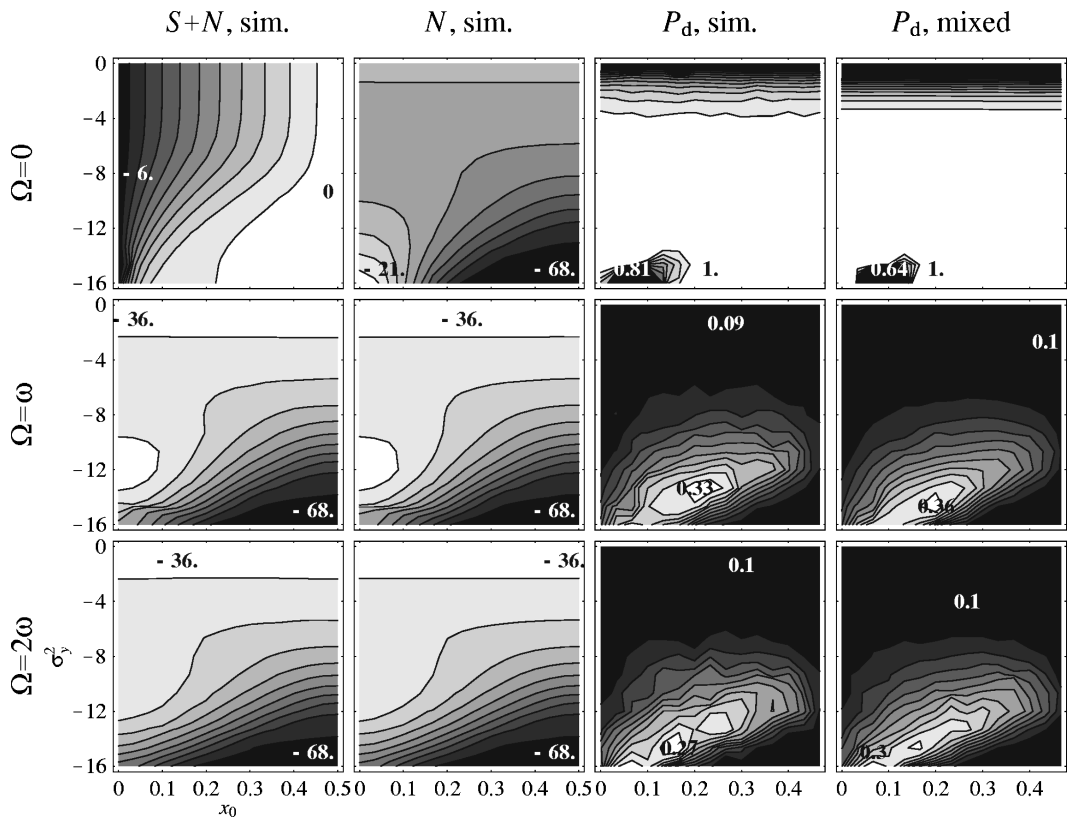

FIG. 5. Same as Fig. 3, with $A=0$.

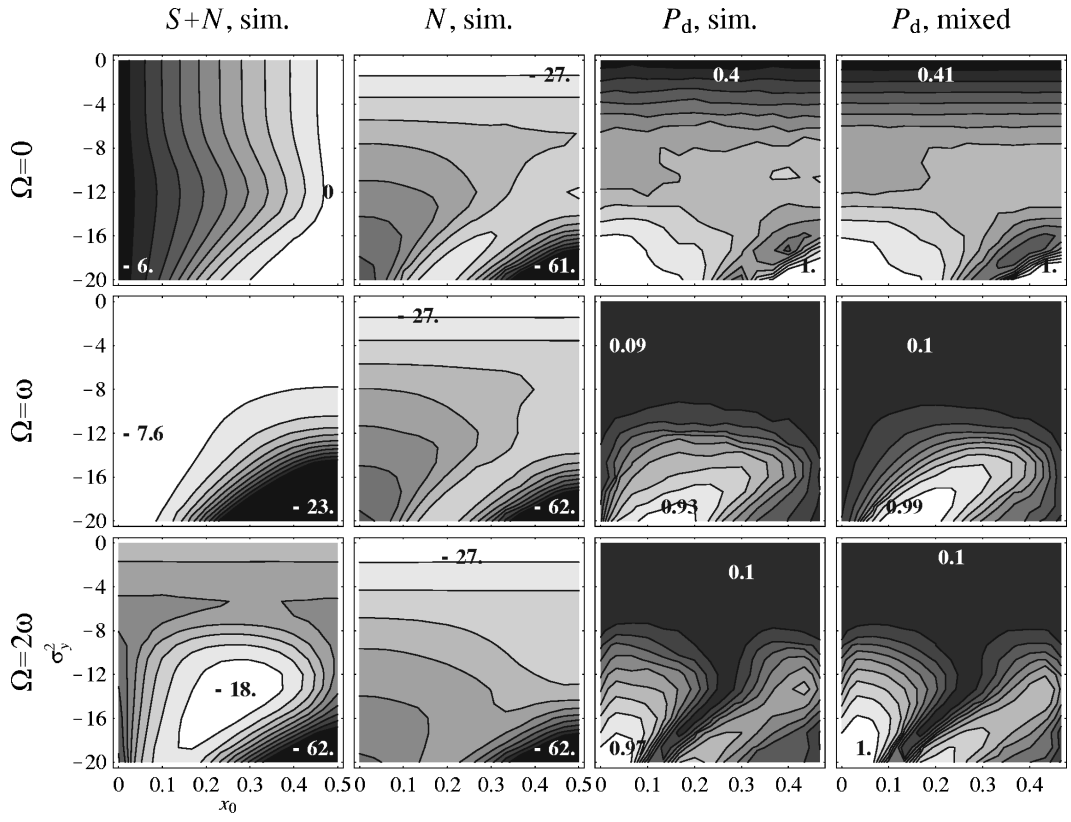

FIG. 6. Same as Fig. 3 with $A=0.56$, $\Delta\omega=\omega/32$, and $T=20.1$ sec.

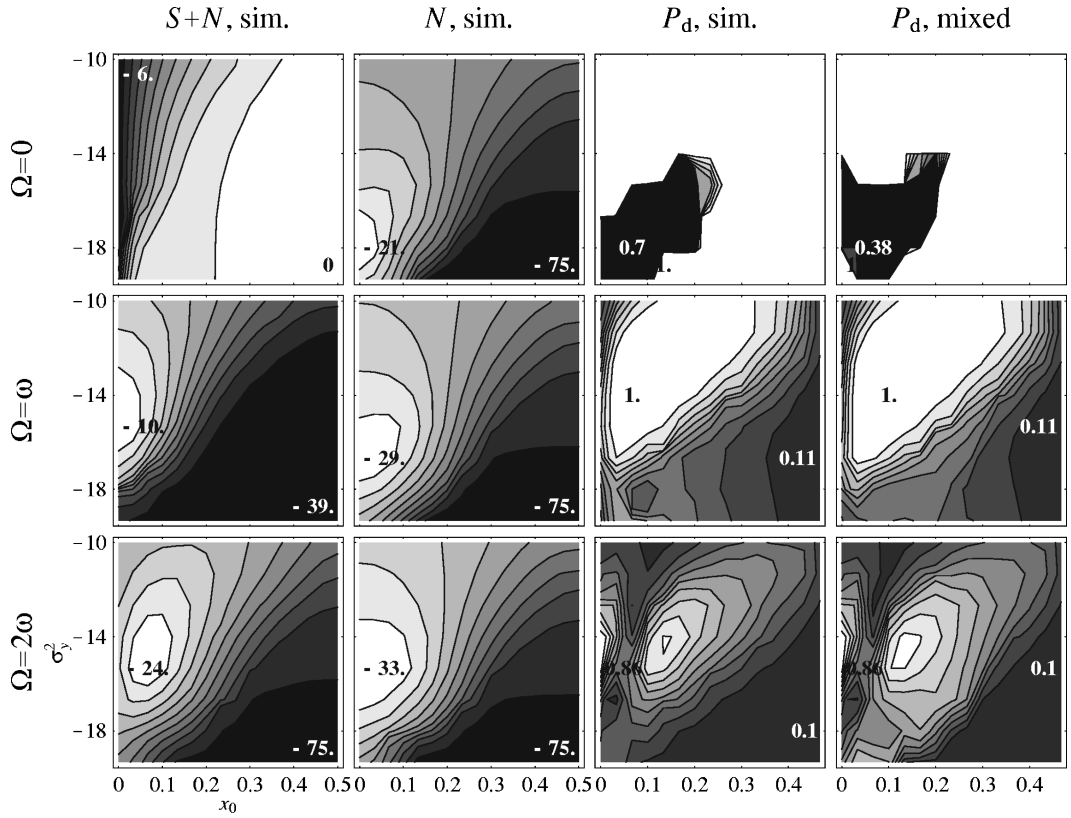

FIG. 7. Same as Fig. 3 with $\tau_c = 0.0005$, $\Delta\omega = \omega/32$, and $T = 20.1$ sec.

VI. CONCLUDING REMARKS

Stochastic resonance, when carefully invoked, can enhance the response of an *a priori nonlinear* detector. Even when the detector is nonlinear, however, a knowledge of the signal detection statistics and their behavior under the conditions of SR is essential before one can consider a practical implementation. In our earlier publications [6,7], we computed the signal detection statistics for a different bistable dynamical device under the ''classical'' SR scenario. The results clearly showed that there was an optimal noise value at which the detection probability (for a fixed false alarm rate) was maximized. However, when the number of adjustable parameters in the system is increased, the system has to be optimized in a higher dimensional space, and it is clear [3] that there exist regimes wherein the response can be significantly degraded; hence, a computation of the signal detection statistics in the space of adjustable parameters becomes critical. As in our earlier work [3], the theoretical results agree very well with simulations in the framework of the adiabatic and perturbation-theoretic approximations used.

In this paper we have studied a nonlinear ''mixing'' or ''heterodyning'' scheme. The scheme affords a technique whereby weak dc (or ac—we defer consideration of this case to a future publication) target signals are made more detectable by ''mixing'' them with a *known* ac bias signal in the nonlinear dynamic device. While we have used the rf SQUID (in a continuation of our previous work [3]) as the example device for calculational purposes, the results of this paper apply to a large class of devices characterized by dynamics of the form (2), which involve bi- or multistable potential energy functions with adjustable asymmetry. The output PSD consists of signal peaks (in theory, delta functions; in practice, they have a finite width) superimposed on a noise background. The heights of the peaks (and the attendant SNR's) are very sensitive to even small changes in the target dc signal, so that one can compute detection probabilities by observing changes in the heights of well-defined deterministic features that are already *above* the noise background, whereas the false alarm rate is set by the noise background. Clearly, this technique affords the possibility of greatly enhanced detectability by providing a means of ''moving'' the target signal into a more acceptable band of the output PSD via a careful selection of the bias frequency ω.

Unresolved issues which may need to be addressed in the context of specific applications include the effects of correlations between the noise and the ac bias signal. Further, the

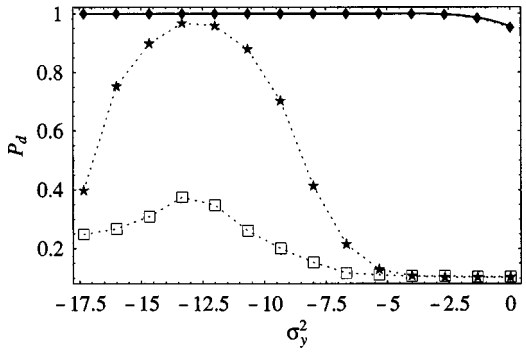

FIG. 8. Detection probability P_d for a fixed false alarm probability of $P_f = 0.1$, maximized over dc bias x_0, using a detector measuring total output power at frequencies $\Omega = 0$ (diamonds), ω (stars), and 2ω (boxes), plotted as a function of noise variance σ_y^2 (in dB). Solid curve: P_d for optimal linear detector. Parameter values: same as Fig. 3.

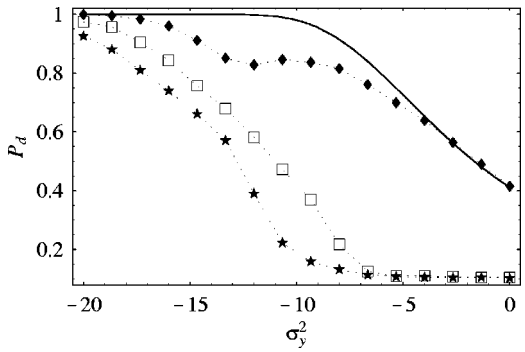

FIG. 9. Same as Fig. 8 with $A=0.56$, $\Delta\omega=\omega/32$, and $T=20.1$ s.

choice of bias signal amplitude and frequency predicate the minimum observation time T for getting acceptable performance. For a given target signal and background noise (these quantities are usually inaccessible to the experimenter), setting the amplitude of the bias signal to be just shy of the deterministic switching threshold and selecting a bias frequency high enough so that the target data are collected over many cycles of the bias signal will yield the shortest observation times for obtaining acceptable performance. In many practical applications one does not have the luxury of collecting large time series from the target, i.e., T is small, so that a careful selection of the bias amplitude and frequency are critical to good performance.

ACKNOWLEDGMENTS

A.R.B. acknowledges support from the Office of Naval Research through Grant No. N0001496AF00002 as well as the Internal Research program at SPAWAR and NATO-CRG 131464. M.E.I. was supported in part by a grant from the DoD CHSSI high performance computing initiative in Computational Electronics and Nanoelectronics. We acknowledge the Department of Defense High Performance Computing Modernization Program for computer time allocations on the CEWES and NAVO Cray T3E supercomputers.

APPENDIX

Here we list the definitions of the constants used in Eqs. (11) and (12):

$$C_1\equiv-\frac{\alpha\overline{\gamma}-\overline{\alpha}\gamma}{4\alpha^2}+\frac{\beta(\alpha\overline{\beta}-\overline{\alpha}\beta)}{4\alpha(\alpha^2+\omega^2)},\quad C_2\equiv\frac{\alpha\beta^2[(2\delta_{s_01}-1)\alpha+\overline{\alpha}]+\omega^2(\alpha\overline{\gamma}-\overline{\alpha}\gamma)}{4\alpha^2\omega^2},\quad C_3\equiv-\frac{\gamma[(2\delta_{s_01}-1)\alpha+\overline{\alpha}]}{4\alpha}.$$

$$a_1\equiv\alpha,\quad b_1\equiv\omega,\quad c_1\equiv-\frac{\alpha\overline{\beta}-\overline{\alpha}\beta}{2\alpha(\alpha^2+\omega^2)}.$$

$$b_2\equiv-\frac{\beta[(2\delta_{s_01}-1)\alpha+\overline{\alpha}]}{2\alpha\omega}.$$

$$a_3\equiv\omega(\alpha\overline{\beta}-\overline{\alpha}\beta),\quad b_3\equiv\alpha\beta[(2\delta_{s_01}-1)\alpha+\overline{\alpha}]+\omega^2[(2\delta_{s_01}-1)\beta+\overline{\beta}],\quad c_3\equiv\frac{1}{2\omega(\alpha^2+\omega^2)}.$$

$$a_4\equiv\alpha^2[\beta(\alpha\overline{\beta}-\overline{\alpha}\beta)-\alpha(\alpha\overline{\gamma}-\overline{\alpha}\gamma)]+\omega^2[-2\beta(\alpha\overline{\beta}-\overline{\alpha}\beta)-\alpha(\alpha\overline{\gamma}-\overline{\alpha}\gamma)],$$

$$b_4\equiv\alpha\omega[3\beta(\alpha\overline{\beta}-\overline{\alpha}\beta)-2\alpha(\alpha\overline{\gamma}-\overline{\alpha}\gamma)]-2\omega^3(\alpha\overline{\gamma}-\overline{\alpha}\gamma),$$

$$c_4\equiv\frac{1}{4\alpha(\alpha^2+\omega^2)(\alpha^2+4\omega^2)}.$$

$$a_5\equiv-a_3,\quad b_5\equiv-b_3,\quad c_5\equiv\frac{\beta c_3}{\omega}.$$

$$a_6\equiv\beta^2,\quad b_6\equiv\gamma\omega,\quad c_6\equiv-\frac{(2\delta_{s_01}-1)\alpha+\overline{\alpha}}{8\alpha\omega^2}.$$

$$a_7\equiv-\alpha\beta^2[(2\delta_{s_01}-1)\alpha+\overline{\alpha}]-2\omega^2\{2\beta[(2\delta_{s_01}-1)\beta+\overline{\beta}]-(\alpha\overline{\gamma}-\overline{\alpha}\gamma)\},$$

$$b_7 \equiv \omega\{2\beta(\alpha\overline{\beta}-\overline{\alpha}\beta)+\alpha\gamma[(2\delta_{s_0 1}-1)\alpha+\overline{\alpha}]+4\omega^2[(2\delta_{s_0 1}-1)\gamma+\overline{\gamma}]\},$$

$$c_7 \equiv \frac{1}{8\omega^2(\alpha^2+4\omega^2)}.$$

[1] For a good overview see P. Jung, Phys. Rep. **234**, 175 (1994).

[2] R. Bartussek, P. Jung, and P. Hänggi, Phys. Rev. E **49**, 3930 (1994); P. Jung and R. Bartussek, in *Fluctuations and Order: The New Synthesis*, edited by M. Millonas (Springer-Verlag, New York, 1996).

[3] A. Bulsara, M. Inchiosa, and L. Gammaitoni, Phys. Rev. Lett. **77**, 2162 (1996); M. Inchiosa, A. Bulsara, and L. Gammaitoni, Phys. Rev. E **55**, 4049 (1997).

[4] For good overviews see K. Wiesenfeld and F. Moss, Nature (London) **373**, 33 (1995); A. Bulsara and L. Gammaitoni, Phys. Today **49** (3), 39 (1996); L. Gammaitoni, P. Hänggi, P. Jung, and F. Marchesoni, Rev. Mod. Phys. **70**, 1 (1998).

[5] See, e.g., H. van Trees, *Detection, Estimation and Modulation Theory* (J. Wiley, New York, 1978).

[6] M. Inchiosa, A. Bulsara, J. Lindner, B. Meadows, and W. Ditto, in *Proceedings of the Third Technical Conference on Nonlinear Dynamics (Chaos) and Full Spectrum Processing*, edited by R. A. Katz (American Institute of Physics, New York, 1995).

[7] M. E. Inchiosa and A. R. Bulsara, Phys. Rev. E **53**, 2021R (1996).

[8] A. Barone and G. Paterno, *Physics and Applications of the Josephson Effect* (J. Wiley, New York, 1982).

[9] A. Hibbs, A. Singsaas, E. Jacobs, A. Bulsara, J. Bekkedahl, and F. Moss, J. Appl. Phys. **77**, 2582 (1995).

[10] *New Type of Magnetic Flux Sensor Based on Stochastic Resonance in a Flux Quantized Superconducting Loop*, Naval Command, Control and Ocean Surveillance Center Technical Document No. 2931 (1996); R. Rouse, S. Han, and J. Lukens, Appl. Phys. Lett. **66**, 108 (1995).

[11] See e.g., C. Gardiner, *Handbook of Stochastic Methods* (Springer-Verlag, Berlin, 1983).

[12] M. Inchiosa, A. Bulsara, A. Hibbs, and B. Whitecotton, Phys. Rev. Lett. **80**, 1381 (1998).

[13] B. McNamara and K. Wiesenfeld, Phys. Rev. A **39**, 4854 (1989).

[14] R. McDonough and A. Whalen, *Detection of Signals in Noise* (Academic Press, San Diego, 1995).

[15] Although $A=0$, we still mention ω as a reminder that our adiabatic approach restricts us to studying the response at frequencies much less than τ_c^{-1}.

[16] L. Gammaitoni, E. Menichaella-Saetta, S. Santucci, F. Marchesoni, and C. Presilla, Phys. Rev. A **40**, 2114 (1989).

[17] P. Hänggi, P. Jung, C. Zerbe, and F. Moss, J. Stat. Phys. **70**, 25 (1993).

[18] M. J. Buckingham, *Noise in Electronic Devices and Systems* (J. Wiley, New York, 1983).

[19] T. Zhou and F. Moss, Phys. Rev. A **41**, 4255 (1990); L. Kiss, Z. Gingl, Z. Marton, J. Kertesz, F. Moss, G. Schmera, and A. Bulsara, J. Stat. Phys. **70**, 451 (1993); V. Shneidman, P. Jung, and P. Hänggi, Phys. Rev. Lett. **72**, 2682 (1994); Europhys. Lett. **26**, 571 (1994); L. Gammaitoni, F. Marchesoni, E. Menichaella-Saetta, and S. Santucci, Phys. Rev. E **51**, R3799 (1995).